2-D Finite-Element Modeling of Surface Dielectric Barrier Plasma Discharge Devices to Understand the Influence of Design Parameters on Sterilization Applications

Arnesh K. Bose[®], *Graduate Student Member, IEEE*, Dinesh Maddipatla[®], *Member, IEEE*, and Massood Z. Atashbar[®], *Senior Member, IEEE*

Abstract—In this study, voltage distribution and surface dielectric barrier discharge (DBD) of a microplasma discharge device (MDD) were modeled in 2-D domain using finite-element analysis (FEA). Initially, the voltage distribution across comb-, H-tree-, and honeycomb-structured MDD was analyzed. Then, the cross section of an MDD consisting of a polyimide-based dielectric sandwiched between two copper electrodes was used for modeling the microplasma discharge characteristics in an argon environment. A sinusoidal voltage was applied to one of the copper electrodes while the other electrode was grounded. The spatial distributions of electron temperature (ET) across the electrodes for varying input voltages were simulated to demonstrate the importance of breakdown voltage. A detailed analysis on the effect of varying electrode and dielectric barrier thicknesses on electron density and ET was also performed to understand the importance of optimizing device configurations for microplasma discharge. Moreover, MDD was also simulated in varying ambient temperature and pressure conditions to evaluate their effect on ET and density across the electrodes. The results from these simulations provide a better understanding of parameters such as varying input voltage, electrode, and dielectric thickness on ET and electron density. This enables us to optimize design parameters for fabricating MDDs and the operating conditions for effective sterilization applications.

Index Terms—2-D simulation, electron density, electron temperature (ET), finite-element analysis, microplasma, surface dielectric barrier discharge (DBD).

I. INTRODUCTION

PLASMA is one of the fundamental states of matter in which gaseous matter undergoes ionization resulting in charge separation, forming positively charged atoms and free electrons [1]. In other words, plasma is a collection of charged particles (electrons and ions) and excited elements formed

Manuscript received March 2, 2021; revised November 1, 2021; accepted February 14, 2022. This work was supported by EArly-Concept Grant for Exploratory Research (EAGER) Grant, National Science Foundation (NSF), under Grant 1917144. The review of this article was arranged by Senior Editor J. L. Lopez. (Corresponding author: Arnesh K. Bose.)

The authors are with the Electrical and Computer Engineering Department, Western Michigan University, Kalamazoo, MI 49008 USA (e-mail: arneshkumar.bose@wmich.edu).

Color versions of one or more figures in this article are available at https://doi.org/10.1109/TPS.2022.3156031.

Digital Object Identifier 10.1109/TPS.2022.3156031

under high temperature or electric field to generate high electron energy. When such conditions of high temperature and high electric field are no longer applied to plasma, electrons recombine with ions, returning the plasma to its neutral gaseous state. Plasma is used in biomedical applications such as sterilization and disinfection, automobile manufacturing processes, environmental remediation, ultraviolet lamps, and space propulsion. Plasma discharge characteristics are generally dependent on the pressure-distance product (pd), where p is the ambient pressure and d is the distance between the two electrodes [2]. The voltage required to ignite/generate the plasma is called the breakdown voltage. The ambient pressure of the plasma discharge and electrode distance is directly related to the breakdown voltage. For example, if d is constant and p is increased to represent a high-pressure environment, it can lead to unstable plasma discharge due to uncontrollable plasma arc formation from filamentation, which is not desirable. On the other hand, if p is kept constant and d is increased to several centimeters, it would increase the breakdown voltage to ignite the plasma [2]. Depending on the ambient pressure conditions, high breakdown voltage can lead to high current density in the cathode region which eventually leads to the formation of uncontrollable plasma arcs [3]. To alleviate such high breakdown voltages, stable nonthermal plasma (NTP) such as microplasma can be ignited under ambient or lower pressure condition (≤ 1 atm) by reducing the electrode gap distance.

Plasma can generally be categorized as thermal and NTP [4], [5]. The thermal plasma is also called as equilibrium plasma (tend to exist in equilibrium state) since the temperature of electrons, ions, and neutrals are almost equal ranging from few thousand Kelvin for a plasma torch to more than a million Kelvin in fusion plasma devices and in the interior of stars. Traditional thermal plasma discharges tend to exist in thermal equilibrium in the bulk plasma where energy distributions for electrons, ions, and neutral particles are assumed to be Maxwellian everywhere, and electrons and ions have the same temperature [1], [5]. In an NTP, the temperature of the electrons is much higher (10000–100000 K) than the temperature of the ions and neutrals, which are

0093-3813 © 2022 IEEE. Personal use is permitted, but republication/redistribution requires IEEE permission. See https://www.ieee.org/publications/rights/index.html for more information.

roughly the same as the room temperature (\sim 300 K) and can range up to about 2500 K [5].

Microplasmas are nonthermal-based plasmas where the plasma discharge is confined spatially to microcavities with dimensions less than 1000 µm exhibiting controllable and stable plasma arcing [6]–[8]. Recently, microplasmas are gaining interest for surface sterilization, ozone synthesis, cancer treatment, water disinfection, toxic analyte detection, surface etching and modification applications, and they have been a major focus of research for developing novel applications in health care, biomedical, food, and environmental industries [5]–[18]. A decadal survey by the National Research Council, Physics 2020/Plasma Science Committee states that the expanding scope of plasma research is creating significant interest and scientific opportunities in NTPs within the fields of chemistry, biology, physics, materials science, and engineering [10]. Traditional thermal and NTP require very high voltage of operation and often operated in special chambers where ambient conditions such as temperature and pressure are continuously monitored and controlled [19], [20]. The major advantage of microplasma discharge device (MDD) lies in the ease of fabrication with various miniaturized configurations, which reduces the breakdown voltage for igniting plasma, requiring relatively smaller transformer and power supply. This increases the possibility to design and fabricate portable MDDs, thus leading to cost efficiency.

The performance of MDDs is dependent on a stable and uniform microplasma discharge. MDD parameters such as electrode gap distance (dielectric thickness), electrode thickness, and applied voltage will affect microplasma discharge characteristics such as electron density ($n_{\rm e}$) and electron temperature (ET) ($T_{\rm e}$) [21]. Moreover, the change in ambient conditions such as temperature and pressure will affect the net $n_{\rm e}$ of the microplasma discharge due to the change in electron mobility ($\mu_{\rm e}$) [22]. Understanding the effect of such variable parameters including electrode and dielectric thickness, applied voltage, and changing ambient conditions will enable us to design effective MDDs based on their operating conditions.

The generation of uniform and effective plasma in MDDs depends on electrode configurations and designs [23]-[31]. It is hypothesized that uniform voltage distribution across the electrodes will result in the generation of uniform n_e and ET, which will lead to uniform, stable, and steady microplasma discharge across the electrode. There are various electrode configurations such as cathode boundary layer (CBL), dielectric barrier discharge (DBD), capillary plasma electrode discharge (CPED), microhollow cathode discharge (MHCD), inverted square pyramidal (ISP), and square cross-sectional cavities (SCSC) [32]. Among these, DBD was identified as the most suitable configuration for fabricating a surface-plasmabased MDD due to its ease of scalability and geometrical flexibility (planar geometry) unlike other configurations [33]–[35]. These devices can operate at atmospheric pressure and temperature with variable input voltage and frequency. Recently, new geometries such as microhollow cathode geometries [33] and plasma pencil geometries have been used to generate microplasma for medical and sterilization purposes [33], [34].

While MDDs using such geometries operate at ambient pressure and temperature, the effective treatment area for each device is very small and is not scalable unlike MDDs that can be made of DBD configuration. Various DBD-based electrode designs including comb, H-tree, and honeycomb were chosen to simulate and study its voltage distribution effect on microplasma discharge of MDDs. Typically, comb structure is selected due to its simplicity [36], and H-tree design is a very common design feature used in the electronics industry to keep the clock frequency and voltage uniform across the printed circuit board [37]. Honeycomb pattern has high surface area and provides uniform voltage and is highly scalable in size and area when compared with the other designs [38].

Various types of surface sterilization have been used to combat antibiotics resistance in microorganisms which is becoming a major problem in conventional medicine, and there is a need to develop alternative technologies to neutralize harmful microorganisms [39]–[47]. Steam sterilization methods require high heat and special chambers for sterilizing microorganisms [48]. Chemical sterilization involves usage of chemicals such as ethyl alcohol, isopropyl alcohol, chlorine compounds, formaldehyde, glutaraldehyde, hydrogen peroxide, peracetic acid, phenolics, ethylene oxide, and ozone and are cost-effective and easy to use when compared with steam sterilizations [49]. However, many of these chemicals are corrosive in high concentration, flammable, and cause eye and skin irritation [49]. To overcome such drawbacks, sterilization using microplasma has been of great interest in research lately, as it provides a low-cost, safe, clean, and more effective alternative to the aforementioned traditional methods [50]. Microplasma-based NTP treatment of microorganisms at room temperature and atmospheric pressure has been shown to reduce the growth of microorganisms such as bacteria on different surfaces such as cloth and metal [43], [44]. The time required for sterilization is on the order of seconds [51], a considerable reduction when compared with the traditional sterilization methods. This time reduction and the capability of sterilization at ambient temperatures and pressures have made microplasma discharges a prospective technology for the future. Active plasma species such as ions, electrons, and ultraviolet radiation can activate, control, and catalyze complex reactions and biochemical processes to sterilize harmful pathogens [52]–[56]. To generate such oxidative stress and kill the bacterium, uniform ionization of gaseous matter is required, and therefore uniform microplasma must be generated across the surface of the electrode.

Microplasma-based finite-element analysis (FEA) simulations have been performed to study electron and ion kinetics and breakdown voltages in coplanar electrode-based microplasma devices [57]–[61]. Some application-specific FEA simulations [62]–[69] were used to study microplasma discharges including plasma thruster [70], [71], material deposition [72], etching processes [73], pollution degradation devices [74], and analytical spectroscopy [75]. Deconinck *et al.* [70] and Shimizu *et al.* [76] performed simulations on microplasma jet-based propulsion device to study the variations in plasma kinetics for various applied voltages and the flow velocity in microcavities, respectively.

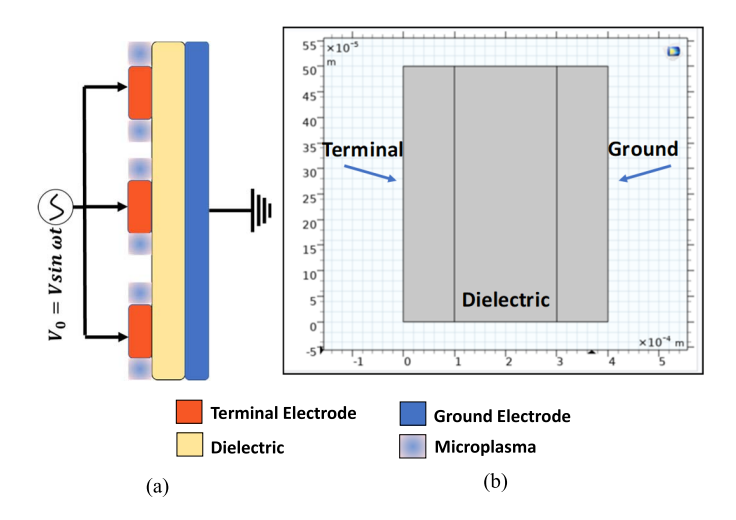


Fig. 1. (a) Schematic of the simplified surface DBD and (b) cross-sectional view of the DBD model in COMSOL simulation software.

Seo and Gary Eden [77] performed simulations of ac-driven DBD microplasma in circular microcavities to understand the effect of cavity diameter on n_e under various ambient pressure conditions. Simulations for microplasma used for additive (printing) and subtractive (etching) manufacturing processes have also been performed by Sawant et al. [72] and Dai et al. [73], respectively, to study the effect of dimensional properties on material deposition and n_e . As microplasmabased sterilization is of growing interest, there is a need to investigate the effect of dielectric and electrode parameters for microplasma discharge. To the best of the authors' knowledge, there is no literature available on 2-D FEA simulations focusing on the effect of electrode and dielectric dimensional parameters on the surface DBD-based microplasma discharges for sterilization applications. Therefore, in this work, the effects of different electrode designs on voltage distribution, varying applied voltages, electrode, and dielectric thickness on n_e and T_e were investigated under ambient conditions such that the breakdown voltage in the discharge medium stays constant to generate stable uniform distribution of microplasma discharge across the surface of the electrodes using COMSOL Multiphysics¹ simulation software.

II. SIMULATION MODEL

DBDs are plasma discharges characterized by the formation of electrical discharges between two conducting electrodes, separated by an insulating material [78]. A sinusoidal voltage is applied to one of the electrodes (terminal electrode) and the other electrode is grounded. Depending on the thickness of the dielectric and/or discharge gap and the discharge medium, the amplitude of the sinusoidal voltage will vary [79]. A schematic of the simplified DBD-based microplasma discharge (side view) and its 2-D model (cross-sectional view) created in COMSOL Multiphysics¹ software along with their different layers are shown in Fig. 1(a) and (b), respectively. Simulation was performed using the Plasma (plas) module in COMSOL Multiphysics¹ which couples the drift diffusion,

heavy species transport, and electrostatics interfaces into an integrated multiphysics interface to model plasma discharges. The model consists of two copper electrodes (ground and terminal electrode) and a polyimide-based dielectric medium. In a surface-based DBD, the thickness of the dielectric between the two electrodes is also referred as the gap distance [8], [9]. The electrodes were separated from each other with a gap distance comprising a dielectric such as polyimide, and a sinusoidal voltage is applied to the terminal electrode [8]. The applied voltage should be high enough to cause ionization of the discharge medium of argon (Ar). The free electrons across the electrodes accelerate and acquire higher potential which leads to electron avalanche, increasing the number of free electrons. The free electrons and the ionized charge species move across the electrode gap to the opposite electrode potential [66]. This process of charge accumulation is temporary, and when the electric field potential is reversed, the process reverses in the opposite direction and repeats as long as the sinusoidal voltage is applied.

The operating principle of the microplasma is based on Paschen's law which states that the breakdown voltage (V_B) of an MDD is a function of the ambient pressure (p) (P_a) and electrode gap distance (d) [80], [81]. The relationship between V_B and p is given by the following equation [80], [81]:

$$V_{\rm B} = \frac{Bpd}{\ln(Apd) - \ln\left[\ln\left(1 + \frac{1}{\gamma_{\rm sc}}\right)\right]} \tag{1}$$

where A is the ionization saturation constant, B is the excitation and ionization energy constant, and $\gamma_{\rm se}$ is the coefficient of secondary electronic emission. Using Paschen's law, the breakdown voltage for microplasma discharge can be calculated. The breakdown voltage and electrode gap distance are some of the most important parameters for an optimized electrode configuration. For high pd values, the applied $V_{\rm B}$ is directly proportional to d [82]. Therefore, if d increases, $V_{\rm B}$ required to dissociate the electrons of the ambient gas (in this work, Ar gas) also increases. A surface-based DBD can also be related to a parallel electrode configuration. From the fundamental laws of electromagnetics, the relationship between electric field and electrode gap distance is given by [83]

$$E = \frac{V}{d} \tag{2}$$

where E is the electric field and V is the potential difference between the parallel conductive plates. When the applied voltage (V) at the terminal electrode is kept constant, it can be derived that E is inversely potential to d. Therefore, if the electrode gap distance increases, the electric field across the two parallel plates will decrease and vice versa. This will affect the electron drift velocity (v_d) , and from the fundamental laws for μ_e in electric field [83]

$$v_{\rm d} = \mu_{\rm e} E \tag{3}$$

where μ_e is the electron mobility. Therefore, v_d is directly proportional to E. According to the kinetic theory of gases, the relationship between v_d and electron temperature T_e is given

¹Trademarked.

by [84]

$$v_{\rm d} = \left(\frac{8k_{\rm b}T_{\rm e}}{\pi m_{\rm e}}\right)^{\frac{1}{2}} \tag{4}$$

where k_b is the Boltzmann's constant, and m_e is the electron mass. According to Maxwellian electron energy distribution function, the effect of T_e on the electron density (n_e) and electron energy density (n_e) is given by [84]

$$T_{\rm e} = \frac{2}{3} \left(\frac{n_{\rm e}}{n_{\rm e}} \right). \tag{5}$$

Therefore, n_e is inversely proportional to T_e and n_e is directly proportional to T_e . T_e must be several orders of magnitude greater than the gas temperature in the discharge medium to be classified as nonequilibrium plasma discharge to maintain lower surface temperature [7]. Therefore, n_e is inversely proportional to T_e if n_e is constant. It can also be inferred that for a constant applied voltage, T_e is inversely proportional to the electrode gap distance (d) (distance between the terminal and the ground electrode). This reduction in T_e will inhibit the microplasma discharge of the device. Similarly, electrode thickness is also an important design parameter for microplasma discharge. The relationship between T_e and electrode layer thickness (d_s) is given by [85]

$$T_{\rm e} = C_1 v_{\rm d} p d_{\rm s}. \tag{6}$$

Therefore, electrode layer thickness (d_s) is directly proportional to T_e . The gap distance between the two electrodes and electrode thickness should be optimized for a lower breakdown voltage allowing for greater operating range of MDD. If the electrode gap distance is not optimized, it would result in low T_e , rendering the MDD ineffective.

Constituent equations from the drift diffusion model (DDM) in COMSOL Multiphysics¹ used for determining n_e for microplasma discharge are mathematically calculated using the following equation [86]:

$$\frac{\partial}{\partial t}(n_{\rm e}) + \nabla \cdot \Gamma_{\rm e} = R_{\rm e} \tag{7}$$

where

$$\Gamma_{e} = -(\mu_{e} \cdot E) n_{e} - \nabla D_{e} n_{e} \tag{8}$$

and n_e denotes n_e (1/m³), R_e is the electron rate expression [1/(m³·s)], μ_e is the electron mobility which is either a scalar or a tensor [m²/(V·s)], E is the electric field (V/m), D_e is the electron diffusivity coefficient (m²/s), and $-(\mu_e \cdot \vec{E})$ n_e and $-\nabla \vec{D}_e n_e$ represent the effect of electric field on electron drift and electron diffusion between high and low n_e , respectively. The effects of n_e and the electric field for varying input voltages across the two electrodes were simulated and investigated. The electric field across the MDD is also a crucial parameter for uniform microplasma discharge. The generation of the reactive species is dependent on n_e and μ_e . Nonuniform electric field across MDD will result in inconsistent generation of reactive species across the electrode, compromising the optimum performance of MDD.

TABLE I REACTIONS OF ELECTRON IMPACT WITH ACTIVE SPECIES OF AR

Reaction	Formula	Туре	ΔE (eV)
R1	$e^- + Ar \rightarrow e^- + Ar$	Elastic Scattering	m/M =
			0.136e-4
R2	$e^- + Ar \rightarrow e^- + Ar^*$	Excitation	11.50
R3	$e^- + Ar \rightarrow e^- + Ar^*$	Superelastic	-11.50
R4	$e^- + Ar \rightarrow 2e^- + Ar^+$	Ionization	15.80
R5	$e^- + Ar^* \rightarrow 2e^- + Ar^+$	Ionization	4.27

Similarly, n_{ε} was determined using the following equation [86]:

$$\frac{\partial}{\partial t}(n_{\varepsilon}) + \nabla \cdot \Gamma_{\varepsilon} + E \cdot \Gamma_{e} = R_{\varepsilon} \tag{9}$$

where

$$\Gamma_{\varepsilon} = -(\mu_{\varepsilon} \cdot \boldsymbol{E}) n_{\varepsilon} - \nabla (\boldsymbol{D}_{\varepsilon} n_{\varepsilon}) \tag{10}$$

and n_{ε} denotes n_{ε} (V/m³), R_{ε} is the energy gain/loss [V/(m³·s)], μ_{ε} is the electron energy mobility which is either a scalar or a tensor [m²/(V·s)], E is the electric field (V/m), D_{ε} is the electron energy diffusivity (m²/s), $-(\mu_{\varepsilon} \cdot \vec{E})n_{\varepsilon}$ and $-\nabla \vec{D}_{\varepsilon}$ n_{ε} represent the effect of electric energy on electron drift and electron diffusion between high and low electron energy density, respectively, and \vec{E} . $\Gamma_{\rm e}$ represents the effect of external electric field on heating of electrons, where heating can be a form of source or sink. Electrons are lost to the dielectric wall due to random motion within a few mean free paths of the wall and are gained later due to secondary emission effects, resulting in the following boundary condition for the electron flux [86]:

$$n.\Gamma_{\rm e} = \left(\frac{1}{2}v_{\rm e}, n_{\rm e}\right) - \sum_{\rm p} \gamma_{\rm p}(\Gamma_{\rm p}.n) \tag{11}$$

and the electron energy flux is given as [86]

$$n.\Gamma_{\varepsilon} = \left(\frac{5}{6}v_{\rm e}, n_{\varepsilon}\right) - \sum_{\rm p} \varepsilon_{\rm p} \gamma_{\rm p} (\Gamma_{\rm p}.n).$$
 (12)

The second term on the right side of (11) is the gain of electrons due to secondary emission effects where γ_p is the secondary emission coefficient. The second term in (12) is the secondary emission energy flux, where ε_p is the mean energy of the secondary electrons.

Using the classical kinetic theory, μ_e is dependent on the change in ambient temperature (T_a) and is mathematically given by the following equation [87]:

$$\mu_{\rm e}N = \frac{4}{3} \frac{e}{(2\pi m)^{\frac{1}{2}} (k_{\rm B} T_{\rm a})^{\frac{5}{2}}} \int_0^\infty \left(\frac{\varepsilon}{\sigma_{\rm mt}(\varepsilon)}\right) e^{-\left(\frac{\varepsilon}{k_{\rm B} T_{\rm a}}\right)} d\varepsilon \qquad (13)$$

where N is the gas density, $\sigma_{\rm mt}$ is the electron-atom momentum transfer scattering cross section, m and e are the electron mass and charge, respectively, and $k_{\rm B}$ is the Boltzmann's constant. Also, as per the ideal gas law [88], since $T_{\rm a}$ and N are dependent on p, it can be inferred that a change in ambient conditions (pressure and/or temperature) should affect $\mu_{\rm e}$ and $n_{\rm e}$.

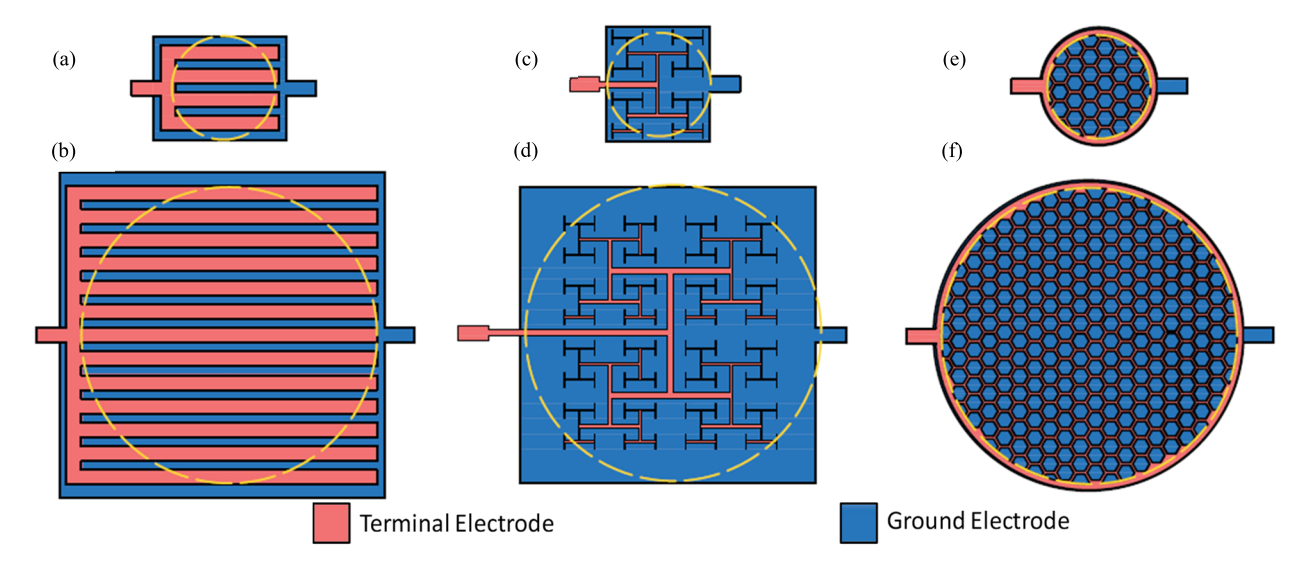


Fig. 2. (a) and (b) Comb-structured MDD; (c) and (d) H-tree-structured MDD; and (e) and (f) honeycomb structured MDD for 35- and 100-mm-diameter standard Petri dishes, respectively. (The doted yellow circle represents the perimeter of the Petri dish, and all the images are not to scale.)

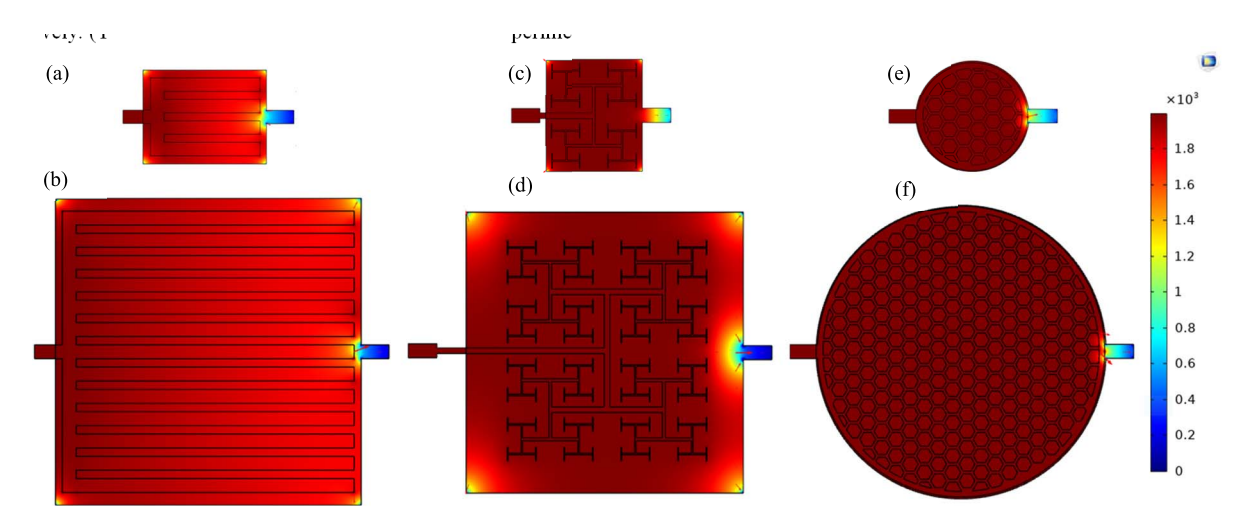


Fig. 3. Simulated voltage distribution across: (a) and (b) comb-structured MDD, (c) and (d) H-tree-structured MDD, and (e) and (f) honeycomb-structured electrodes for 35- and 100-mm-diameter Petri dishes, respectively. (All images are not to scale.)

TABLE II REACTIONS BETWEEN THE ATOMS AND MOLECULES WITH THEIR REACTION RATES

Reaction	Formula	Rate (m³/s.mol)
R6	$Ar^* + Ar^* \rightarrow e^- + Ar + Ar^+$	3.3734e8
R7	$Ar^* + Ar \rightarrow Ar + Ar$	1807

TABLE III SURFACE REACTIONS

Reaction	Formula	Sticking Coefficient
R8	$Ar^+ \rightarrow Ar$	1
R9	$Ar^* \to Ar$	1

The reactions due to electron impact inside the gas gap are given in Tables I and II. The reactions of electron impact with active species of Ar including: metastable argon (Ars),

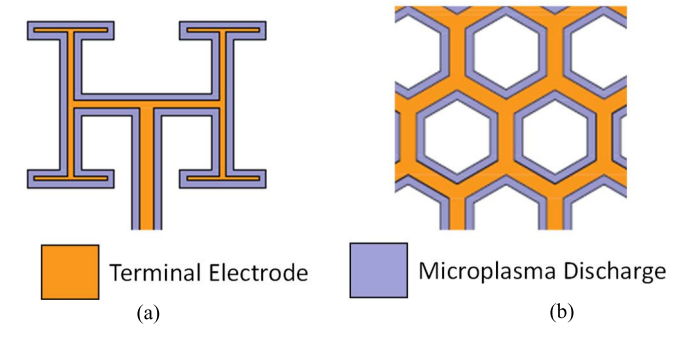


Fig. 4. Illustration of microplasma discharge coverage for: (a) H-tree-structured MDD and (b) honeycomb-structured MDD.

Ar molecule, and singly ionized Ar molecule (Ar+) are depicted in Table I [80], [81]. In Table II, the reaction rates for Ar atoms and molecules along with its corresponding two-body reaction are also given [80], [81], [83]. The surface reactions are also given in Table III. The initial electron

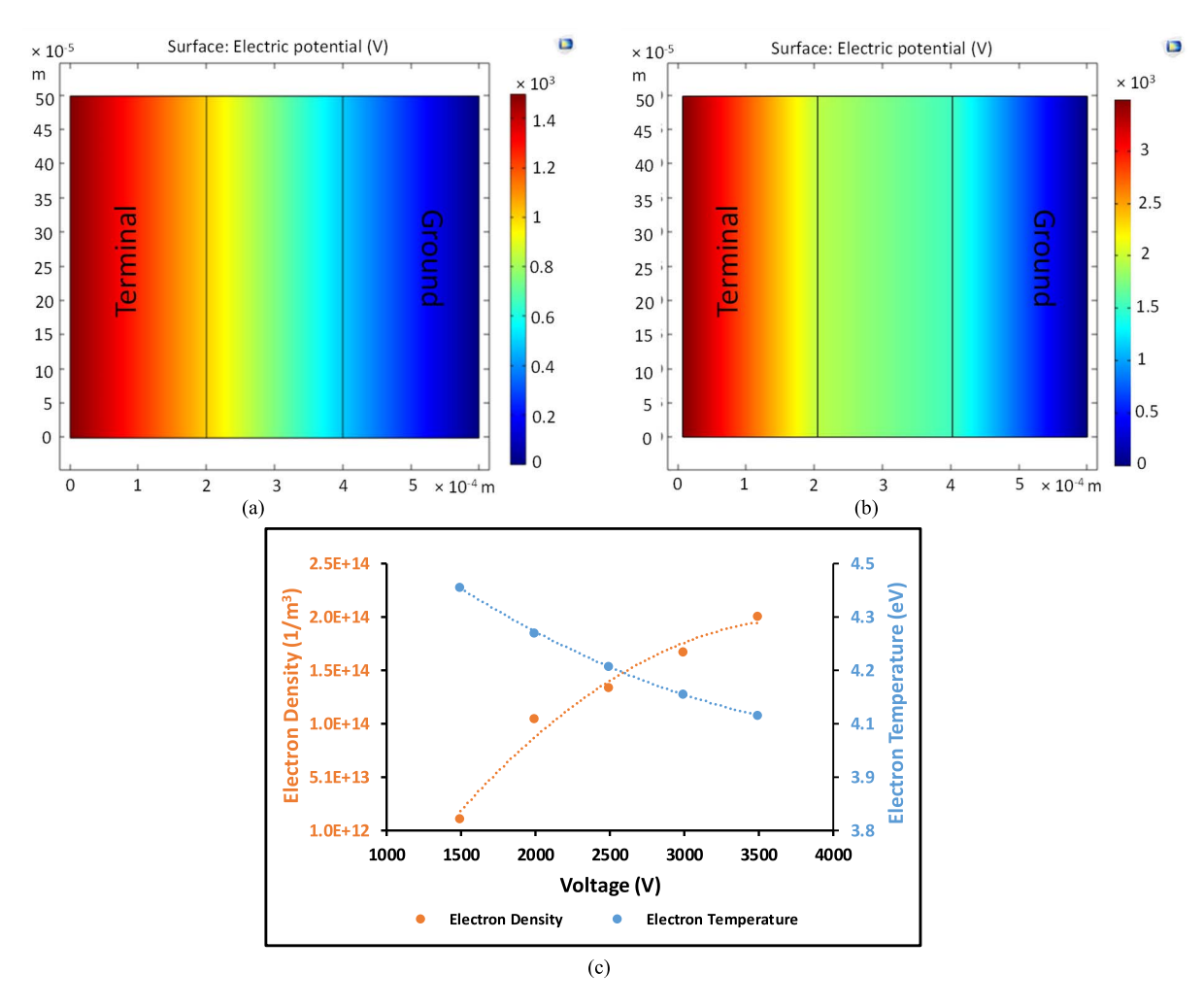


Fig. 5. Electric voltage distribution across layers for an input terminal voltage of: (a) 1500 V; (b) 3500 V; and (c) influence of varying input voltage on electron density and temperature.

density (ε_0) was considered as 10^6 , and the mean electron energy was considered as 4 eV. The ambient temperature and pressure were kept constant at 300 K and 1 atm, respectively; when simulating for voltage distribution, $T_{\rm e}$ and $n_{\rm e}$ for varying electrode and dielectric thickness.

III. SIMULATION RESULTS

Surface microplasma discharges produce reactive species of gas molecules which induces electroporation effect. This facilitates DNA mutation and inhibits DNA repair and enzyme activities, resulting in cellular necrosis and responsible for pathogenic microbial inactivation [39]–[47]. To achieve electroporation effect, the applied voltage to MDD is an important parameter, and the voltage distribution across the device should be uniform for effective sterilization of pathogenic microorganisms. To obtain uniform voltage distribution across electrodes, the design of electrodes is crucial when fabricating MDD. Nonuniform voltage distribution across the device can result in ineffective sterilization. A case study of three different electrode structures was performed, to investigate voltage distribution across electrode. A schematic of the comb-,

H-tree-, and honeycomb-structured MDD for 35- and 100-mm-diameter Petri dishes is shown in Fig. 2. The yellow dotted circle indicates the perimeter of the Petri dishes, to illustrate the coverage of each designed MDD.

A 2-D simulation in FEA software COMSOL Multiphysics¹ was performed using magnetic and electric field modules. An input voltage of 2000 V at 20 kHz was applied to the terminal electrode, and the voltage distribution across different electrode designs to sterilize the surface of 35- and 100-mm Petri dishes was simulated and is shown in Fig. 3. It was observed that for a comb-structured MDD [Fig. 3(a) and (b)], the voltage gradually dropped toward the comb tips by \sim 15%. If the voltage across the comb-structured device decreases, then it will affect microplasma discharge leading to nonuniform microplasma discharge. Such nonuniform voltage distribution will ultimately affect the formation of reactive species throughout the surface of the device, causing ineffective sterilization. However, voltage distribution on the terminal electrode was uniform for H-tree [Fig. 3(c) and (d)] and honeycomb devices [Fig. 3(e) and (f)], with minimal drop (<0.5%) in voltage toward the ground terminal. This results in uniform electric field distribution and leads to uniform microplasma

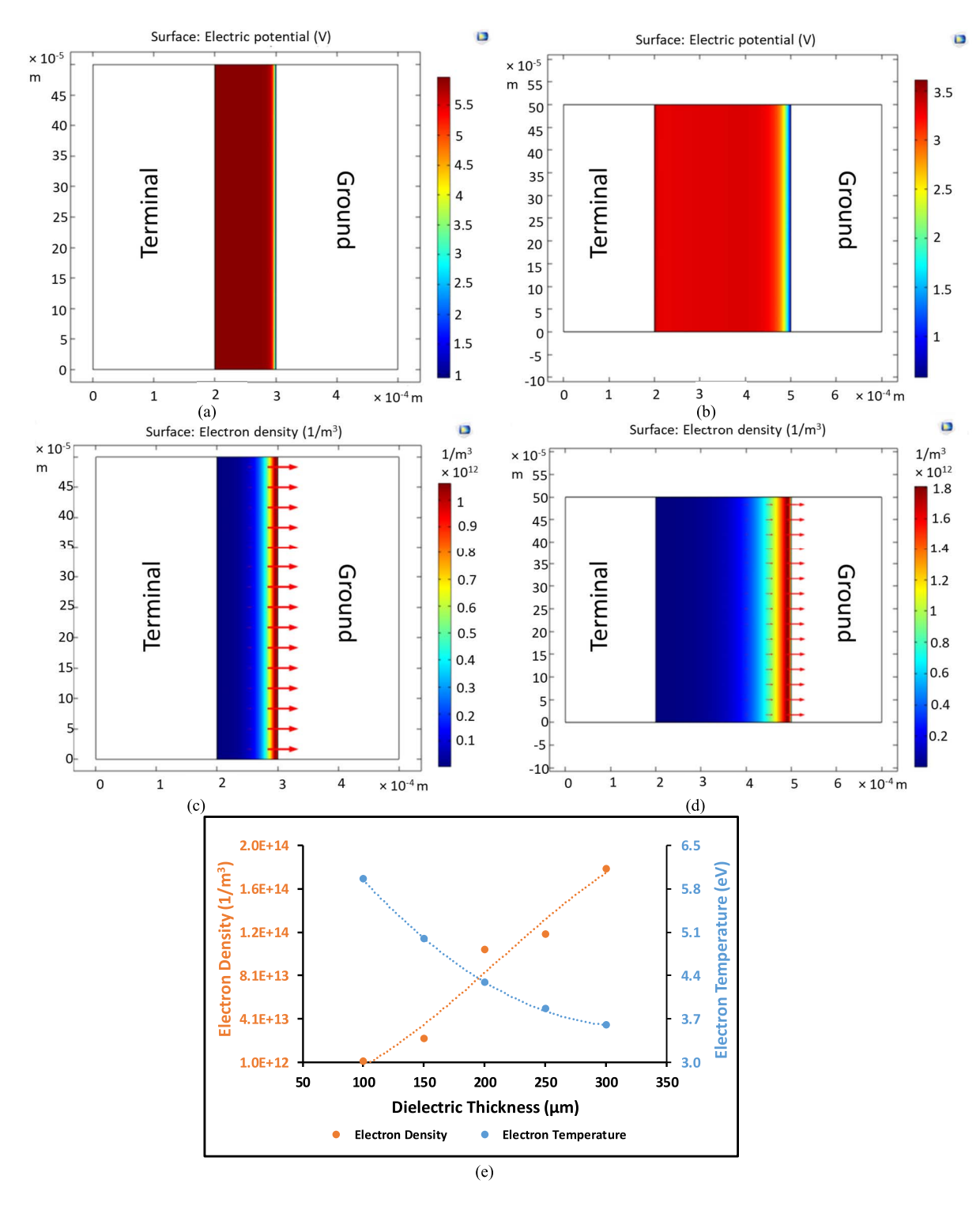


Fig. 6. ET and density distribution across: (a) and (b) 100-µm-thick dielectric and (c) and (d) 300-µm-thick dielectric where arrows indicate the direction of electron flux toward the ground electrode and (e) influence of varying dielectric thickness on electron density and temperature.

discharge throughout the surface of the devices. The voltage distribution across the H-tree-structured device was very similar to honeycomb; however, the coverage of microplasma discharge was very different for both the designs. Considering 0.5-mm (Fig. 4) thick/wide microplasma spread across the terminal electrode, for 35-mm-diameter Petri dish, it was calculated that the H-tree-structured device has $\sim 12\%$ greater

coverage in microplasma discharge when compared with the honeycomb device. However, when MDD was scaled for 100-mm-diameter Petri dish, the honeycomb device has $\sim 55\%$ greater coverage of microplasma discharge when compared with the H-tree device. Therefore, the honeycomb-structured MDD not only has uniform voltage distribution across the terminal electrode but also improves the scalability

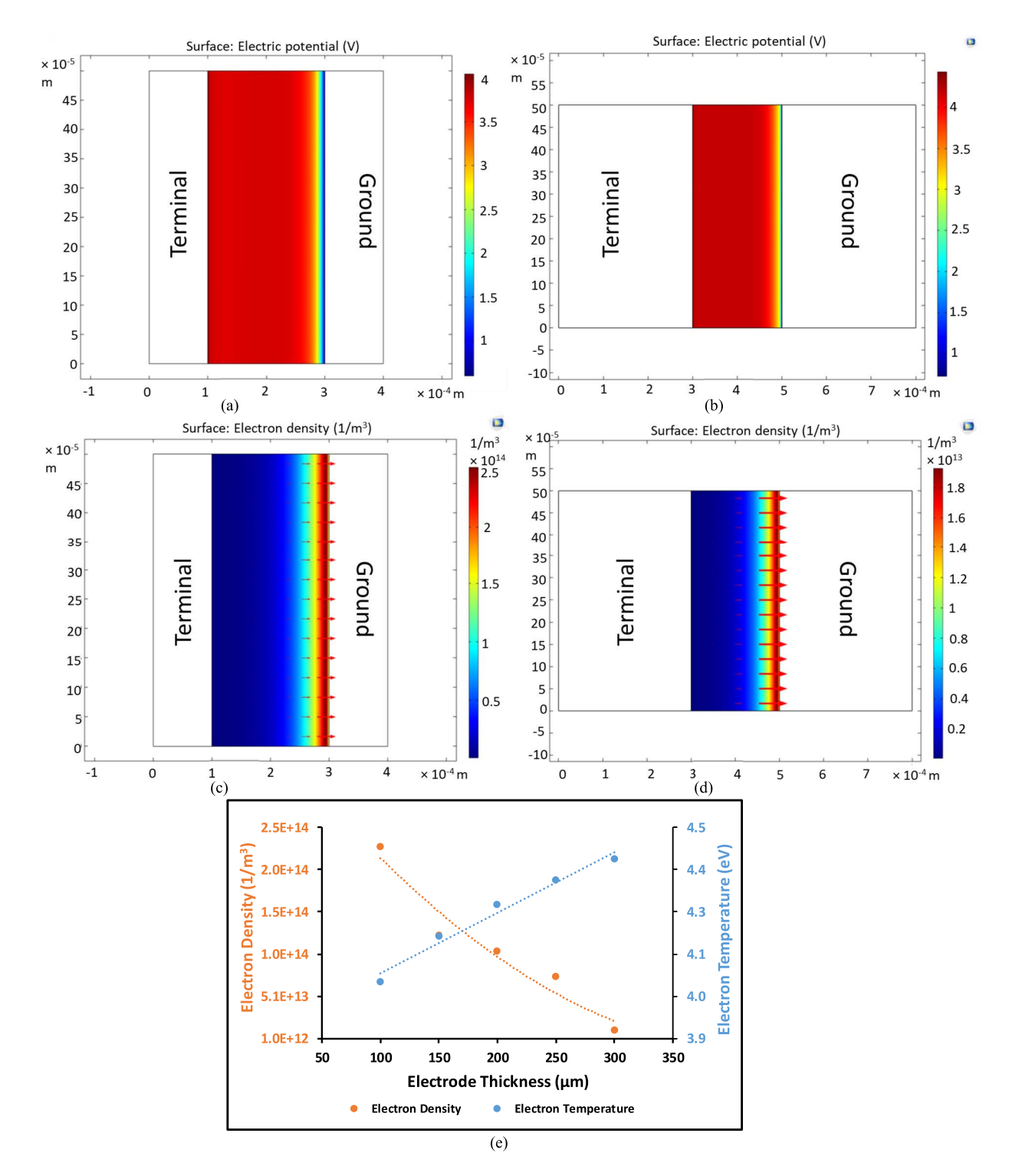
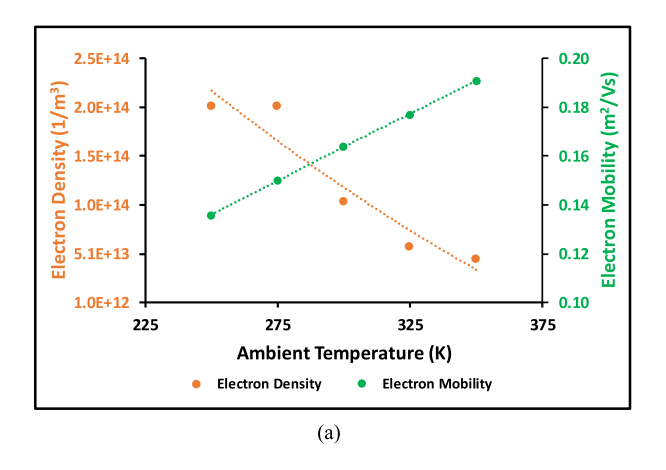


Fig. 7. ET and density distribution across: (a) and (b) 100- μ m-thick electrode and (c) and (d) 300- μ m-thick electrode where arrows indicate the direction of electron flux toward the ground electrode and (e) influence of varying electrode thickness on electron density and temperature.

over the H-tree patterned MDD and provides relatively large microplasma discharge area.

The input sinusoidal voltage at the terminal electrode was varied from 1500 to 3500 V in steps of 500 V, and its effect on $n_{\rm e}$ and $T_{\rm e}$ was investigated. Electric potential distribution across the terminal electrode, dielectric, and ground electrode for 1500 and 3500 V is shown in Fig. 5(a) and (b), respectively.

The thickness of the electrodes and dielectric was considered as 200 μ m, and the voltage distribution across the electrodes was simulated under ambient atmospheric temperature (300 K) and pressure (1 atm). For varying voltages of 1500, 2000, 2500, 3000, and 3500 V, the maximum $T_{\rm e}$ decreased to 4.39, 4.28, 4.20, 4.13, and 4.08 eV, respectively. Similarly, the maximum $n_{\rm e}$ per cubic meter increased to 1.21×10^{13} ,



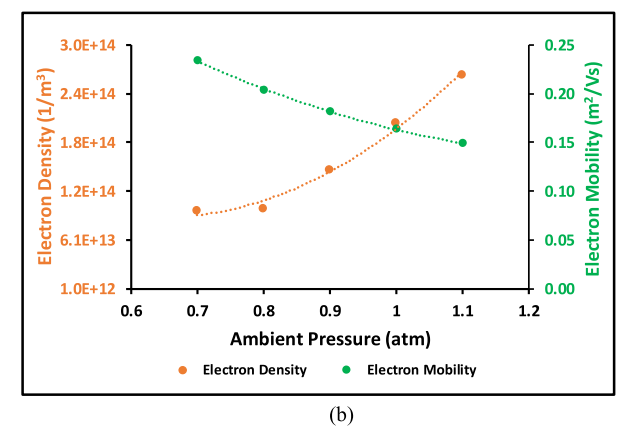


Fig. 8. Influence of varying ambient: (a) temperature and (b) pressure on electron mobility and ET.

 1.05×10^{14} , 1.35×10^{14} , 1.68×10^{14} , and 2.01×10^{14} when the input sinusoidal voltage at the terminal electrode was varied from 1500 to 3500 V, respectively. From Fig. 5(c), it was observed that $T_{\rm e}$ is inversely proportional to $n_{\rm e}$ [also evident from (5)]. In addition, the breakdown voltage for 200- μ m dielectric was observed at approximately 2000 V. If the voltage distribution across the electrodes is uniform and above the breakdown voltage (2000 V) of the dielectric layer, uniform microplasma can be generated across the surface of MDD.

The effect of varying dielectric thickness on $T_{\rm e}$ and $n_{\rm e}$ was investigated. The dielectric thickness was varied from 100 to 300 μ m in steps of 50 μ m with an input sinusoidal voltage of 2000 V at the terminal electrode under ambient atmospheric temperature (300 K) and pressure (1 atm). The simulation results of T_e and n_e distribution for 100- and 300-μm-thick dielectric along with direction of the electron flux are shown in Fig. 6(a)-(d) and plotted in Fig. 6(e), respectively. For dielectric thickness of 100, 150, 200, 250, and 300 μ m, the maximum T_e decreased to 5.95, 4.99, 4.28, 3.86, and 3.59 eV, respectively. Similarly, n_e increased to 0.01 \times $10^{14},\,0.22\times10^{14},\,1.04\times10^{14},\,1.19\times10^{14},\,\text{and}\,\,1.79\times10^{14}$ when the dielectric thickness increased from 100 to 300 μ m, in steps of 50 μ m, respectively. From (2), it is inferred that for a constant voltage at the terminal electrode, the dielectric thickness of a device is inversely proportional to the electric field. The electric field is directly proportional to the drift velocity of the electrons [from (3)]. The drift velocity in turn is proportional to the square root of $T_{\rm e}$ [from (4)]. Correlating (2)-(5), it can be deduced that the electrode gap distance is inversely proportional to $T_{\rm e}$ and directly proportional to $n_{\rm e}$ [from (5)]. Therefore, to achieve similar levels of plasma discharge for increased dielectric thickness, a higher voltage needs to be applied at the terminal electrode to increase $T_{\rm e}$. However, if the input voltage is kept constant as the dielectric thickness increases, then the voltage at the terminal electrode will not be enough to breakdown and dissociate the discharge media, thereby limiting the generation of microplasma.

Similarly, the effect of varying electrode thickness (increased from 100 to 300 μ m in steps of 50 μ m) on $T_{\rm e}$ and $n_{\rm e}$ was investigated with an input sinusoidal voltage

of 2000 V at the terminal electrode under a temperature of 300 K and a pressure of 1 atm [Fig. 7(a)–(e)]. For increasing electrode thickness of 100, 150, 200, 250, and 300 μ m, the maximum ET increased to 4.06, 4.19, 4.28, 4.35, and 4.41 eV, respectively. Similarly, n_e increased to 2.28 × 10¹⁴ m⁻³, 1.23 × 10¹⁴ m⁻³, 1.04 × 10¹⁴ m⁻³, 0.74 × 10¹⁴ m⁻³, and 0.11 × 10¹⁴ m⁻³ when the dielectric thickness increased 100–300 μ m. From (6), it is inferred that T_e is directly proportional to the electrode thickness and, n_e is inversely proportional to the electrode thickness. If the electrode is too thick, the voltage drop across the electrode will be higher and this will result in lower voltages (
breakdown voltage in the discharge medium) across the dielectric. Therefore, the choice of electrode thickness is an important parameter for microplasma discharge.

In Fig. 8(a), the effect of varying ambient temperature on n_e and μ_e is shown. The electrode and dielectric thickness were fixed at 200 μ m with an input sinusoidal voltage of 2000 V at the terminal electrode. It was observed that n_e and $\mu_{\rm e}$ varied from 2.03 \times 10¹⁴ to 4.54 \times 10¹³ m⁻³ and 0.14 to 0.19 $[m^2/(V \cdot s)]$, respectively, as the ambient temperature increased from 250 to 350 K, in steps of 25 K at a constant ambient pressure (1 atm). This corresponds to a 78% and 50% change in n_e and μ_e , respectively. As the atmospheric temperature decreases, μ_e decreases and n_e increases, thereby decreasing $T_{\rm e}$ and vice versa [as per (5)]. Therefore, at lower ambient temperature, the input voltage supply must be increased to maintain constant $T_{\rm e}$ [89]. Similarly, in Fig. 8(b), the effect of varying ambient pressure on n_e and μ_e is shown. The electrode and dielectric thickness were fixed at 200 μ m with an input sinusoidal voltage of 2000 V at the terminal electrode. It was observed that n_e and μ_e varied from 9.64 \times 10¹³ to $2.64 \times 10^{14} \text{ m}^{-3}$ and 0.23 to 0.15 [m²/(V·s)], respectively, as the ambient temperature increased from 0.7 to 1.1 atm, in steps of 0.1 atm at a constant ambient temperature (300 K). This corresponds to a 174% and 36% change in n_e and μ_e , respectively. The results indicate that n_e is inversely proportional to μ_e for varying atmospheric pressure conditions. When the atmospheric pressure increases, μ_e reduces, thereby reducing T_e [as per (3) and (4)]. To maintain T_e constant, the input voltage can be increased, which would also increase the

collisional energy transfer between electrons and background gas [90], [91]. Therefore, it can be concluded that the change in $n_{\rm e}$ and $\mu_{\rm e}$ due to the variations in the ambient conditions will have a direct effect on microplasma discharge, influencing the sterilization efficacy of MDD toward harmful pathogens.

IV. CONCLUSION

In this work, an MDD was successfully modeled and simulated using FEA in COMSOL Multiphysics¹ simulation software. Initially, the voltage distribution across comb-, H-tree-, and honeycomb-structured MDDs was analyzed to find the optimum design for microplasma discharge. The results indicate that the honeycomb-structured MDD provides uniform voltage distribution and relatively larger microplasma coverage when compared with comb- and H-treestructured MDDs. The cross section of an MDD was modeled in an Ar environment with a polyimide dielectric sandwiched between two copper electrodes. Simulations were performed to investigate $n_{\rm e}$ and electric field distribution for ac terminal voltages ranging from 1500 to 3500 V with a constant dielectric and electrode thickness of 200 μ m. Then, the effect of varying dielectric and electrode thickness parameters on n_e and temperature was investigated. As the dielectric thickness increased from 100 to 300 μ m, T_e decreased by almost 40%. The results indicate that it is necessary to have a thinner dielectric between the two copper electrodes for lower breakdown voltage and effective microplasma discharge. The varying electrode thickness from 100 to 300 μ m resulted in a 9% increase of T_e . This was because T_e is directly proportional to electrode thickness. The results from 2-D modeling indicate that electrode configuration is an important parameter to optimize for fabricating MDDs. For lightweight and wearable applications, it is essential to have thinner electrode and dielectric such that the device is flexible and conformal enough. Finally, the effect of varying ambient temperature and pressure on n_e and mobility of the MDD was studied. A variation of 78% and 50% change in n_e and μ_e was obtained as the ambient temperature was increased from 240 to 360 K at constant ambient pressure (1 atm), respectively. A variation of 174% and 36% change in n_e and μ_e was obtained as the ambient pressure increased from 0.7 to 1.1 atm at constant ambient temperature (300 K), respectively. It was observed that a change in n_e and μ_e will affect the microplasma discharge which in turn can affect the sterilizing efficacy of MDD. Therefore, further research includes developing an adaptive system such that the input voltage can change depending on the varying ambient conditions to generate consistent microplasma discharge. The system will be developed and tested, to sterilize surfaces from harmful Gram-negative and Gram-positive bacteria such as Escherichia coli, Pseudomonas aeruginosa, Staphylococcus aureus, and Bacillus subtilis.

REFERENCES

- [1] F. F. Chen, "Introduction to plasma physics and controlled fusion volume 1: Plasma physics," *Phys. Today*, vol. 38, p. 87, Jan. 1985.
- [2] D. Mariotti, J. A. McLaughlin, and P. Maguire, "Experimental study of breakdown voltage and effective secondary electron emission coefficient for a micro-plasma device," *Plasma Sources Sci. Technol.*, vol. 13, no. 2, p. 207, 2004.

- [3] S. Ramakrishnan and M. W. Rogozinski, "Properties of electric arc plasma for metal cutting," *J. Phys. D: Appl. Phys.*, vol. 30, no. 4, p. 636, 1997.
- [4] X. Cai, X. Wei, and C. Du, "Thermal plasma treatment and coprocessing of sludge for utilization of energy and material," *Energy Fuels*, vol. 34, no. 7, pp. 7775–7805, Jul. 2020.
- [5] D. Mariotti and R. M. Sankaran, "Microplasma for nanomaterials synthesis," J. Phys. D: Appl. Phys., vol. 43, no. 32, 2010, Art. no. 323001.
- [6] J. G. Eden et al., "Plasma science and technology in the limit of the small: Microcavity plasmas and emerging applications," IEEE Trans. Plasma Sci., vol. 41, no. 4, pp. 661–675, Apr. 2013.
- [7] R. Foest, M. Schmidt, and K. Becker, "Microplasmas, an emerging field of low-temperature plasma science and technology," *Int. J. Mass Spectrometry*, vol. 248, no. 3, pp. 87–102, Feb. 2006.
- [8] K. H. Schoenbach and K. Becker, "20 years of microplasma research: A status report," Eur. Phys. J. D, vol. 70, p. 29, Feb. 2016.
- [9] C.-C. Hsu, J.-H. Tsai, Y.-J. Yang, Y.-C. Liao, and Y.-W. Lu, "A foldable microplasma-generation device on a paper substrate," *J. Microelectro*mech. Syst., vol. 21, no. 5, pp. 1013–1015, Oct. 2012.
- [10] National Academies of Sciences, Engineering, and Medicine, Plasma Science: Enabling Technology, Sustainability, Security, and Exploration, National Academies Press, Washington, DC, USA, 2020.
- [11] K. H. Becker, K. H. Schoenbach, and J. G. Eden, "Microplasmas and applications," J. Phys. D: Appl. Phys., vol. 39, no. 3, pp. R55–R70, Feb. 2006.
- [12] J. Foster, B. Sommers, B. Weatherford, B. Yee, and M. Gupta, "Characterization of the evolution of underwater DBD plasma jet," *Plasma Sources Sci. Technol.*, vol. 20, no. 3, Jun. 2011, Art. no. 034018.
- [13] S. K. Pankaj et al., "Applications of cold plasma technology in food packaging," Trends Food Sci. Technol., vol. 35, no. 1, pp. 5–17, Jan. 2014.
- [14] M. Keidar et al., "Cold atmospheric plasma in cancer therapy," Phys. Plasmas, vol. 20, no. 5, 2013, Art. no. 57101.
- [15] G. Isbary et al., "Reasons why we need cold atmospheric plasmas in bacteria-related diseases in medicine," Plasma Med., vol. 2, nos. 1–3, pp. 85–96, 2012.
- [16] A. K. Bose, D. Maddipatla, B. B. Narakathu, B. J. Bazuin, and M. Z. Atashbar, "Laser-assisted patterning of a flexible microplasma discharge device for heavy metal and salt detection in ambient air," in *Proc. IEEE Int. Conf. Flexible Printable Sensors Syst. (FLEPS)*, Jul. 2019, pp. 1–3.
- [17] S. Dou, L. Tao, R. Wang, S. El Hankari, R. Chen, and S. Wang, "Plasma-assisted synthesis and surface modification of electrode materials for renewable energy," *Adv. Mater.*, vol. 30, no. 21, May 2018, Art. no. 1705850.
- [18] A. K. Bose, D. Maddipatla, B. B. Narakathu, S. Hajian, B. J. Bazuin, and M. Z. Atashbar, "Laser-assisted patterning of a flexible microplasma discharge device for heavy metal and salt detection in ambient air," in *Proc. IEEE Int. Conf. Flexible Printable Sensors Syst. (FLEPS)*, Glasgow, U.K., Jul. 2019, p. 31.
- [19] R. Radjef, K. Jarvis, B. L. Fox, and S. L. McArthur, "Design and characterization of a plasma chamber for improved radial and axial film uniformity," *Plasma Processes Polym.*, vol. 17, no. 8, Aug. 2020, Art. no. 2000017.
- [20] J. Han et al., "Three-dimensional measurements of plasma parameters in an inductively coupled plasma processing chamber," Phys. Plasmas, vol. 26, no. 10, Oct. 2019, Art. no. 103503.
- [21] E. C. B. B. Aragão et al., "Low temperature microplasma jet at atmospheric pressure for inducing surface modification on polyethylene substrates," Amer. J. Condens. Matter Phys., vol. 4, no. 3A, pp. 1–7, Jun. 2014.
- [22] P. Bruggeman and R. Brandenburg, "Atmospheric pressure discharge filaments and microplasmas: Physics, chemistry and diagnostics," *J. Phys. D: Appl. Phys.*, vol. 46, no. 46, Nov. 2013, Art. no. 464001.
- [23] Y. Song et al., "An atmospheric-pressure large-area diffuse surface dielectric barrier discharge used for disinfection application," *IEEE Trans. Plasma Sci.*, vol. 43, no. 3, pp. 821–827, Mar 2015
- [24] S. B. Karki, E. Yildirim-Ayan, K. M. Eisenmann, and H. Ayan, "Miniature dielectric barrier discharge nonthermal plasma induces apoptosis in lung cancer cells and inhibits cell migration," *BioMed Res. Int.*, vol. 2017, pp. 1–12, Jan. 2017.
- [25] O. J. Lee et al., "An experimental burn wound-healing study of non-thermal atmospheric pressure microplasma jet arrays," J. Tissue Eng. Regenerative Med., vol. 10, no. 4, pp. 348–357, 2016.

- [26] H. Yamazaki, T. Ohshima, Y. Tsubota, H. Yamaguchi, J. A. Jayawardene, and Y. Nishimura, "Microbicidal activities of low frequency atmospheric pressure plasma jets on oral pathogens," *Dental Mater. J.*, vol. 30, no. 3, pp. 384–391, 2011.
- [27] A. Rahman et al., "Absolute UV and VUV emission in the 110–400 nm region from 13.56 MHz driven hollow slot microplasmas operating in open air," Plasma Sources Sci. Technol., vol. 13, no. 3, p. 537, 2004.
- [28] C. Lazzaroni and P. Chabert, "A comparison between micro hollow cathode discharges and atmospheric pressure plasma jets in Ar/O₂ gas mixtures," *Plasma Sources Sci. Technol.*, vol. 25, no. 6, Oct. 2016, Art. no. 065015.
- [29] Y. C. Hong, H. J. Park, B. J. Lee, W.-S. Kang, and H. S. Uhm, "Plasma formation using a capillary discharge in water and its application to the sterilization of E. coli," *Phys. Plasmas*, vol. 17, no. 5, May 2010, Art. no. 053502.
- [30] T.-S. Cho, S.-H. Park, K. H. Becker, and E. E. Kunhardt, "Investigation of discharge phenomena in microscale capillary plasma electrode discharges," *IEEE Trans. Plasma Sci.*, vol. 39, no. 6, pp. 1496–1499, Jun. 2011.
- [31] A. Huynh et al., "Nonequilibrium plasma decontamination of corn steep liquor for ethanol production: SO₂ removal and disinfection," Plasma Med., vol. 6, nos. 3–4, pp. 219–234, 2016.
- [32] A. P. Papadakis, "Microplasmas: A review," Open Appl. Phys. J., vol. 4, no. 1, pp. 45–63, Dec. 2011.
- [33] A. Sakudo, Y. Yagyu, and T. Onodera, "Disinfection and sterilization using plasma technology: Fundamentals and future perspectives for biological applications," *Int. J. Mol. Sci.*, vol. 20, no. 20, p. 5216, Oct. 2019.
- [34] J. Winter, R. Brandenburg, and K.-D. Weltmann, "Atmospheric pressure plasma jets: An overview of devices and new directions," *Plasma Sources Sci. Technol.*, vol. 24, no. 6, Oct. 2015, Art. no. 064001.
- [35] U. Kogelschatz, B. Eliasson, and W. Egli, "Dielectric-barrier discharges. Principle and applications," *Le J. de Phys. IV*, vol. 7, no. C4, pp. C4-47–C4-66, Oct. 1997.
- [36] X. Zhang, A. Bose, D. Maddipatla, B. Narakathu, V. Turkani, and M. Atashbar, "Design, simulation and fabrication of a novel MEMS based pulsometer," *Proceedings*, vol. 2, no. 13, p. 951, Dec. 2018.
- [37] M. E. Moses, S. Forrest, A. L. Davis, M. A. Lodder, and J. H. Brown, "Scaling theory for information networks," J. R. Soc. Interface, vol. 5, no. 29, pp. 1469–1480, 2008.
- [38] H. Kim and S. Lee, "Characterization of electrical heating of graphene/PLA honeycomb structure composite manufactured by CFDM 3D printer," Fashion Textiles, vol. 7, no. 1, pp. 1–18, Dec. 2020.
- [39] G. Isbary et al., "Reasons why we need cold atmospheric plasmas in bacteria-related diseases in medicine," Plasma Med., vol. 2, nos. 1–3, pp. 85–96, 2012.
- [40] H. Eto, Y. Ono, A. Ogino, and M. Nagatsu, "Low-temperature sterilization of wrapped materials using flexible sheet-type dielectric barrier discharge," *Appl. Phys. Lett.*, vol. 93, no. 22, Dec. 2008, Art. no. 221502.
- [41] K.-D. Weltmann et al., "Antimicrobial treatment of heat sensitive products by miniaturized atmospheric pressure plasma jets (APPJs)," J. Phys. D: Appl. Phys., vol. 41, no. 19, Oct. 2008, Art. no. 194008.
- [42] Z. S. Rad and F. A. Davani, "Non-thermal atmospheric pressure dielectric barrier discharge plasma source construction and investigation on the effect of grid on wound healing application," *Clin. Plasma Med.*, vol. 4, no. 2, pp. 56–64, Dec. 2016.
- [43] C. V. Suschek and C. Opländer, "The application of cold atmospheric plasma in medicine: The potential role of nitric oxide in plasma-induced effects," *Clin. Plasma Med.*, vol. 4, no. 1, pp. 1–8, Jul. 2016.
- [44] R. López-Callejas et al., "Alternative method for healing the diabetic foot by means of a plasma needle," Clin. Plasma Med., vol. 9, pp. 19–23, Mar. 2018.
- [45] X. Liao et al., "Inactivation mechanisms of non-thermal plasma on microbes: A review," Food Control, vol. 75, pp. 83–91, May 2017.
- [46] N. Y. Babaeva and G. V. Naidis, "Modeling of plasmas for biomedicine," Trends Biotechnol., vol. 36, no. 6, pp. 603–614, Jun. 2018.
- [47] X. Su et al., "Inactivation efficacy of nonthermal plasma-activated solutions against Newcastle disease virus," Appl. Environ. Microbiol., vol. 84, no. 9, May 2018, Art. no. e02836.
- [48] X. Li and M. Farid, "A review on recent development in nonconventional food sterilization technologies," *J. Food Eng.*, vol. 182, pp. 33–45, Aug. 2016.

- [49] J.-H. Yoo, "Review of disinfection and sterilization—Back to the basics," Infection Chemotherapy, vol. 50, no. 2, p. 101, 2018.
- [50] M. Moisan, J. Barbeau, S. Moreau, J. Pelletier, M. Tabrizian, and L. Yahia, "Low-temperature sterilization using gas plasmas: A review of the experiments and an analysis of the inactivation mechanisms," *Int. J. Pharmaceutics*, vol. 226, nos. 1–2, pp. 1–21, 2001.
- [51] A. K. Bose, C. L. Beaver, B. B. Narakathu, S. Rossbach, B. J. Bazuin, and M. Z. Atashbar, "Development of flexible microplasma discharge device for sterilization applications," in *Proc. IEEE Sensors*, Oct. 2018, pp. 1–4.
- [52] M. Krewing, B. Schubert, and J. E. Bandow, "A dielectric barrier discharge plasma degrades proteins to peptides by cleaving the peptide bond," *Plasma Chem. Plasma Process.*, vol. 40, no. 3, pp. 685–696, May 2020.
- [53] P. Bourke, D. Ziuzina, L. Han, P. J. Cullen, and B. F. Gilmore, "Microbiological interactions with cold plasma," *J. Appl. Microbiol.*, vol. 123, no. 2, pp. 308–324, Aug. 2017.
- [54] F. Iza et al., "Microplasmas: Sources, particle kinetics, and biomedical applications," Plasma Process. Polym., vol. 5, no. 4, pp. 322–344, Jun. 2008.
- [55] K. Pai et al., "Investigation of the roles of plasma species generated by surface dielectric barrier discharge," Sci. Rep., vol. 8, no. 1, pp. 1–13, Dec. 2018.
- [56] A. L. Santos et al., "Effects of UV-B radiation on the structural and physiological diversity of bacterioneuston and bacterioplankton," Appl. Environ. Microbiol., vol. 78, no. 6, pp. 2066–2069, Mar. 2012.
- [57] J. Choi, F. Iza, J. K. Lee, and C. M. Ryu, "Electron and ion kinetics in a DC microplasma at atmospheric pressure," *IEEE Trans. Plasma Sci.*, vol. 35, no. 5, pp. 1274–1278, Oct. 2007.
- [58] Y. J. Hong, S. M. Lee, G. C. Kim, and J. K. Lee, "Modeling high-pressure microplasmas: Comparison of fluid modeling and particle-in-cell Monte Carlo collision modeling," *Plasma Process. Polym.*, vol. 5, no. 6, pp. 583–592, 2008.
- [59] M. U. Lee, S. Y. Jeong, I. H. Won, S. K. Sung, G. S. Yun, and J. K. Lee, "Non-maxwellian to Maxwellian transitions of atmospheric microplasmas at microwave frequencies," *Phys. Plasmas*, vol. 23, no. 7, Jul. 2016, Art. no. 070704.
- [60] H. Y. Kim, M. Gołkowski, C. Gołkowski, P. Stoltz, M. B. Cohen, and M. Walker, "PIC simulations of post-pulse field reversal and secondary ionization in nanosecond argon discharges," *Plasma Sources Sci. Technol.*, vol. 27, no. 5, May 2018, Art. no. 055011.
- [61] L.-G. Meng, J.-P. Xing, Y.-J. Lv, Z.-H. Liang, and C.-L. Liu, "Simulations of breakdown voltage of coplanar electrodes microplasma devices," *IEEE Trans. Plasma Sci.*, vol. 41, no. 1, pp. 12–16, Jan. 2013.
- [62] M. Z. Atashbar, B. J. Bazuin, M. Simpeh, and S. Krishnamurthy, "3D FE simulation of H2 SAW gas sensor," Sens. Actuators B, Chem., vols. 111–112, pp. 213–218, Nov. 2005.
- [63] A. Bose, B. Narakathu, B. Bazuin, and M. Atashbar, "Modelling and simulation of microplasma discharge device for sterilization applications," *Multidisciplinary Digit. Publishing Inst. Proc.*, vol. 2, no. 13, p. 948, 2018.
- [64] M. Z. Atashbar, B. J. Bazuin, and S. Krishnamurthy, "Design and simulation of SAW sensors for wireless sensing," in *Proc. IEEE Sensors*, vol. 1, Oct. 2003, pp. 584–589.
- [65] M. Z. Atashbar and W. Wlodarski, "Design, simulation and fabrication of doped TiO₂-coated surface acoustic wave oxygen sensor," *J. Intell. Mater. Syst. Struct.*, vol. 8, no. 11, pp. 953–959, Nov. 1997.
- [66] S. Krishnamurthy, M. Z. Atashbar, and K. Kalantar-Zadeh, "3D modeling and simulation of SH-SAW devices using the finite element method," in *IEEE Sensors*, pp. 357–359, 2007.
- [67] C.-J. Cheng and M. Z. Atashbar, "Finite element simulation of SMFBAR based sensor," in *Proc. IEEE Int. Conf. Electro/Inf. Technol.*, Jun. 2009, pp. 190–195.
- [68] C. J. Cheng and M. Z. Atashbar, "Three dimensional finite element modeling and simulation of quasi-shear mode resonator based on c-axistitled ZnO film," in *Proc. IEEE Sensors*, Oct. 2009, pp. 1072–1076.
- [69] M. Z. Atashbar, B. J. Bazuin, and S. Krishnamurthy, "Performance evaluation of SAW devices by simulation," *Int. J. Model. Simul.*, vol. 24, no. 4, pp. 250–262, 2005.

- [70] T. Deconinck, S. Mahadevan, and L. L. Raja, "Computational simulation of coupled nonequilibrium discharge and compressible flow phenomena in a microplasma thruster," *J. Appl. Phys.*, vol. 106, no. 6, Sep. 2009, Art. no. 063305.
- [71] T. Takahashi, Y. Takao, K. Eriguchi, and K. Ono, "Numerical and experimental study of microwave-excited microplasma and micronozzle flow for a microplasma thruster," *Phys. Plasmas*, vol. 16, no. 8, Aug. 2009, Art. no. 083505.
- [72] M. S. Sawant, N. K. Jain, and S. H. Nikam, "Theoretical modeling and finite element simulation of dilution in micro-plasma transferred arc additive manufacturing of metallic materials," *Int. J. Mech. Sci.*, vol. 164, Dec. 2019, Art. no. 105166.
- [73] Y. Dai, L. Wen, J. Liu, and H. Wang, "Simulation and experiment of inverted pyramid DBD micro-plasma devices array for maskless nanoscale etching," in *Proc. IEEE 11th Annu. Int. Conf. Nano/Micro Eng. Mol. Syst. (NEMS)*, Apr. 2016, pp. 460–463.
- [74] J. Mizeraczyk, B. Hrycak, M. Jasiński, and M. Dors, "Low-temperature microwave microplasma for bio-decontamination," *Przeglad Elek-trotechniczny*, vol. 88, no. 9, pp. 238–241, 2012.
- [75] T. Martens, A. Bogaerts, W. Brok, and J. van Dijk, "Computer simulations of a dielectric barrier discharge used for analytical spectrometry," *Anal. Bioanal. Chem.*, vol. 388, no. 8, pp. 1583–1594, Aug. 2007.
- [76] K. Shimizu, M. Yoshinori, I. Akihiko, and B. Marius, "Microplasma actuator for active flow control: Experiment and simulation," in *Proc. JJAP Conf.*, vol. 4, Oct. 2015, pp. 1–9.
- [77] J. H. Seo and J. G. Eden, "Two-dimensional simulation of AC-driven microplasmas confined to 100–300μm diameter cylindrical microcavities in dielectric barrier devices," J. Appl. Phys., vol. 100, no. 12, Dec. 2006, Art. no. 123302.
- [78] R. Brandenburg, "Dielectric barrier discharges: Progress on plasma sources and on the understanding of regimes and single filaments," *Plasma Sources Sci. Technol.*, vol. 26, no. 5, Mar. 2017, Art. no. 053001.
- [79] U. Kogelschatz, "Dielectric-barrier discharges: Their history, discharge physics, and industrial applications," *Plasma Chem. Plasma Process.*, vol. 23, no. 1, pp. 1–46, 2003.
- [80] L. F. Berzak, S. E. Dorfman, and S. P. Smith, Paschen's Law in Air and Noble Gases. Berkeley, CA, USA: Lawrence Berkeley National Laboratory, 2006.
- [81] R. Massarczyk, P. Chu, C. Dugger, S. R. Elliott, K. Rielage, and W. Xu, "Paschen's law studies in cold gases," *J. Instrum.*, vol. 12, no. 6, Jun. 2017, Art. no. P06019.
- [82] Y. Fu, P. Zhang, J. P. Verboncoeur, and X. Wang, "Electrical break-down from macro to micro/nano scales: A tutorial and a review of the state of the art," *Plasma Res. Exp.*, vol. 2, no. 1, Feb. 2020, Art. no. 013001.
- [83] C. Canali, C. Jacoboni, F. Nava, G. Ottaviani, and A. Alberigi-Quaranta, "Electron drift velocity in silicon," *Phys. Rev. B Condens. Matter*, vol. 12, no. 6, p. 2265, 1975.
- [84] Plasma Module. COMSOL Multiphysics. Accessed: Feb. 17, 2020.
 [Online]. Available: https://doc.comsol.com/5.3/doc/com.comsol.help.plasma/PlasmaModuleUsersGuide.pdf
- [85] V. A. Lisovsky, "Electron temperature dependence on electrode layer characteristics in low-pressure RF discharge," in *Proc. Int. Conf. Plasma Sci. (Papers Summary Form Only Received)*, 1995, p. 145.
- [86] Dielectric Barrier Discharge. COMSOL Multiphysics. Accessed: Feb. 22, 2021. [Online]. Available: https://www.comsol.com/model/dielectric-barrier-discharge-8637
- [87] A. F. Borghesani and P. Lamp, "Electron mobility in dense argon gas at several temperatures," *IEEE Trans. Dielectr. Electr. Insul.*, vol. 10, no. 6, pp. 977–984, Dec. 2003.
- [88] A. Laugier and J. Garai, "Derivation of the ideal gas law," J. Chem. Educ., vol. 84, no. 11, p. 1832, 2007.
- [89] F. Su, W. Wang, A. G. Burns, X. Yue, and F. Zhu, "The correlation between electron temperature and density in the topside ionosphere during 2006–2009," *J. Geophys. Res. Space Phys.*, vol. 120, no. 12, pp. 10,724–10,739, 2015.
- [90] A. P. Rao, M. Gragston, A. K. Patnaik, P. S. Hsu, and M. B. Shattan, "Measurement of electron density and temperature from laser-induced nitrogen plasma at elevated pressure (1-6 bar)," *Opt. Exp.*, vol. 27, no. 23, pp. 33779–33788, 2019.
- [91] S. C. Schaub, J. S. Hummelt, W. C. Guss, M. A. Shapiro, and R. J. Temkin, "Electron density and gas density measurements in a millimeter-wave discharge," *Phys. Plasmas*, vol. 23, no. 8, Aug. 2016, Art. no. 083512.



Arnesh K. Bose (Graduate Student Member, IEEE) received the B.Tech. degree from the West Bengal University of Technology, Kolkata, India, in 2013, and the M.S. degree from the University of Kansas, Lawrence, KS, USA, in 2016. He is currently pursuing the Ph.D. degree in electrical engineering with Western Michigan University, Kalamazoo, MI, USA.

He was a Teaching Assistant with the Department of Electrical and Computer Engineering, College of Engineering and Applied Sciences,

Western Michigan University, where he was also a Research Assistant with the Center for Advanced Smart Sensors and Structures, Department of Electrical and Computer Engineering. He is currently working as an Electrical Engineer II with SAF-Holland, Inc., Muskegon, MI, USA, and is part of the Global Innovation Group, Muskegon, developing sensor systems for use in automotive applications. His current work includes analog sensor development, integrating sensor systems in vehicle, prototyping next-generation sensor systems, electrical machinery, electric drive and regeneration, and applications engineering for commercial heavy tractor-trailer industry. His other research interests include design, fabrication, and characterization of printed sensors, 3-D printing, laser-assisted patterning of thin films, flexible microplasma discharge devices, surface sterilization of biofilms, plasma-based liquid media sterilization, and optical-based electrochemical sensing.



Dinesh Maddipatla (Member, IEEE) received the B.E. degree in electrical and electronics engineering from Anna University, Chennai, India, in 2013, the M.Sc. degree in electrical engineering from Western Michigan University, Kalamazoo, MI, USA, in 2016, and the Ph.D. degree from the Electrical and Computer Engineering Department, Western Michigan University, in 2020.

He is currently working as a Research Associate with the Centre for Advanced Smart Sensors and Structures (CASSS), Western Michigan University.

He has authored over 100 refereed journal articles and refereed conference proceedings. In addition, he has over 15 patent applications and invention disclosures. His research interests include all aspects of design, fabrication, and characterization of printed electronics focusing on flexible sensor structures, microfluidics, electrochemical sensors, gas sensors, and lab-on-a-chip sensing systems.

Dr. Maddipatla was awarded the Technology Transfer Talent Network (T3N) from the State of Michigan, the All-University Research and Creative Scholar Award, and the Dissertation Completion Fellowship from Western Michigan University. He is also serving as a reviewer for more than 15 international journals.



Massood Z. Atashbar (Senior Member, IEEE) received the B.Sc. degree in electrical engineering from the Isfahan University of Technology, Isfahan, Iran, in 1989, the M.Sc. degree in electrical engineering from the Sharif University of Technology, Tehran, Iran, in 1989, and the Ph.D. degree from the Department of Communication and Electronic Engineering, Royal Melbourne Institute of Technology University, Melbourne, VIC, Australia, in 1992.

From 1998 to 1999, he was a Post-Doctoral Fellow with the Center for Electronic Engineering

and Acoustic Materials, Pennsylvania State University, State College, PA, USA. He is currently a Presidential Innovation Professor, a Professor with the Electrical and Computer Engineering Department, and the Founding Director of the Center for Advanced Smart Sensors and Structures (CASSS), Western Michigan University, Kalamazoo, MI, USA. He has authored over 290 refereed articles, refereed conference proceedings, and four book chapters. In addition, he has authored ten patents and more than 35 intellectual disclosures. His research interests include physical and chemical sensor development, wireless sensors, and nanotechnology applications in sensors and flexible hybrid electronic devices.

Dr. Atashbar is serving as a Lead Member of the Technical Council Committee and the Co-Chair of the Technical Working Group (TWG) for NextFlex, a DoD-Funded Consortium for Flexible Hybrid Electronics. He was a Guest Editor of *MDPI Biosensors Journal* for a special issue on Printed and Flexible Sensors. He served as an Associate Editor for the IEEE SENSORS JOURNAL from 2006 to 2016.